Astronomy & Astrophysics manuscript no. AA
October 7, 2022

Research on the quantity and brightness evolution characteristics of Photospheric Bright Points groups

HaiCheng Bai[1], Peng Yang[2], Limin Zhao[1], and Yang Yang[1,⋆]

[1] Ynunan Normal University, School of Physics and Electronic Information, Kunming, Yunnan 650500, China
[2] Ynunan Normal University, School of Information, Kunming, Yunnan 650500, China

October 7, 2022

ABSTRACT

Context. Photospheric bright points (BPs), as the smallest magnetic element of the photosphere and the footpoint tracer of the magnetic flux tube, are of great significance to the study of BPs. Compared with the study of the characteristics and evolution of a few specific BPs, the study of BPs groups can provide us with a better understanding of the characteristics and overall activities of BPs groups.
Aims. We aim to find out the evolution characteristics of the brightness and number of BPs groups at different brightness levels, and how these characteristics differ between quiet and active regions.
Methods. We propose a hybrid BPs detection model (HBD Model) combining traditional technology and neural network. The Model is used to detect and calculate the BPs brightness characteristics of each frame of continuous high resolution image sequences of active and quiet regions in TiO-band of a pair of BBSO. Using machine learning clustering method, the PBs of each frame was divided into four levels groups (level1-level4) according to the brightness from low to high. Finally, Fourier transform and inverse Fourier transform are used to analyze the evolution of BPs brightness and quantity in these four levels groups.
Results. The activities of BPs groups are not random and disorderly. In different levels of brightness, their quantity and brightness evolution show complex changes. Among the four levels of brightness, BPs in the active region were more active and intense than those in the quiet region. However, the quantity and brightness evolution of BPs groups in the quiet region showed the characteristics of large periodic changes and small periodic changes in the medium and high brightness levels (level3 and level4). The brightness evolution of PBs group in the quiet region has obvious periodic changes, but the active region is in a completely random and violent fluctuation state.

Key words. Techniques: image processing – Sun:photosphere– Sun: activity– methods: analytical

1. Introduction

Photospheric bright points (BPs) are small, bright structures on the solar photosphere, usually appearing in the intergranule lanes. A BPs is the result of the constant interaction between a magnetic flux tube and the photosphere, so it can be considered as a tracer of the footpoint of magnetic flux tubes in the photosphere (Berger et al. 1998; De Pontieu 2002; M. et al. 2003; Yang et al. 2016). In addition, BPs are pushed into inter-granular lanes, which continuously oscillate under buffeting of granules, and excited magnetohydrodynamic (MHD) waves propagate upward through the flux tube and transfer energy into the chromosphere and and lower corona to heat these regions of the solar atmosphere (Jess et al. 2009; Mumford and Erdélyi 2015; Mumford et al. 2015; Fedun et al. 2010; A. et al. 2011; Vigeesh et al. 2012; Gao et al. 2021). Thus, BPs play a key role in helping to study the various behaviors of magnetic elements in photospheres and explain coronal heating.

Accurate detection of PBs in observed images is an important prerequisite for studying BPs. Some automatic detection methods have been proposed in previous studies, which mainly include typical traditional image techniques and deep learning. Typical traditional techniques generally use the Laplacian operator combined with region growing or morphology methods. Crockett et al. (2009) presented a algorithm that can be used for the automated detection of the BPs in the spatial and temporal domains. The algorithm works by mapping the lanes through intensity thresholding. A compass search, combined with a study of the intensity gradient across the detected objects, allows the disentanglement of BPs from bright pixels within the granules. Feng et al. (2012) calculates candidate seeds using the Laplacian and uses some probabilistic criteria to detect PBs. The method of candidate seed is calculated using (μ+3σ).Where μ and σ are the mean and variance of the image, respectively. Deng (2017) used the Laplacian transform and morphological dilatation algorithm is applied to detect BPs. Xiong et al. (2017) proposed a 3D track-while-detect method to detect and track photosphere BPs and chromosphere BPs, which used 3D method for region growth. Liu (2018) used Laplacian as seed for regional growth to detect BPs. Saavedra et al. (2021) segmented images by multiple thresholds to detect PBs. Deep learning has also been applied to the detection of BPs. Yang and Li (2019) presented a BPs Mask Region-based Convolutional Neural Networks (GBP-MRCNN) for morphological classification of GBPs. Xu et al. (2021) proposed Track region-based Convolutional Neural Networks to detect BPs, and used them to study the characteristics of multiwavelength isolated BPs.

These detection methods have achieved good results. However, there are still some problems.

⋆ Yang Yang is the corresponding authors.
emails: yyang_ynu@163.com

- In traditional algorithms (Feng et al. 2012; Deng 2017; Liu 2018), the image binarization after Laplacian calculation depends on the threshold, and the calculation method using $T = \alpha\mu + \beta\sigma$ is used to calculate the image threshold (where μ and σ are the mean and variance of the image respectively,and α and β are empirical values) will become inaccurate with the change of the observed data.
- It is difficult to control the selection of seed points in the regional growth method, which can easily lead to insufficient or excessive growth, thus causing the problem of missing or multiple detection (Xiong et al. 2017; Liu 2018).
- Using deep learning methods requires the use of annotated datasets, because BPs are too small (some even only a few pixels) and have different shapes, it is difficult to determine the edges when labeling. Therefore, the accuracy of annotated data is difficult to grasp, resulting in the problem of inaccurate edge recognition (Yang and Li 2019; Xu et al. 2021).

Statistical properties describing BPs properties, such as size, brightness, velocity, and lifetime, have been studied extensively using various detection methods. A typical BPs magnetic field is about 1000 Gauss and usually has a point-like or elongated shape. They have an equivalent diameter of about 100-300 km and a lifetime of about 90 seconds to 10 minutes (Berger et al. 1995; Berger and others 1996; Keys et al. 2020). The ratio of the maximum brightness (intensity) of BPs to its mean photosphere brightness is 0.8 – 1.8 in quiet region (Berger et al. 1995). In addition, Crockett et al. (2010) found that the distributions peak at an area of $\approx$ 45,000 km^{-2}, with a sharp decrease toward smaller areas, and the distributions conform with log-normal statistics. Keys et al. (2011) studied the subsequent velocity characteristics of over 6000 structures, finding an average velocity of approximately 1 km s^{-1}, with maximum values of 7 km s^{-1}. Yang et al. (2014) studied the size, brightness and velocity of isolated BPs in five different life stages based on lifespan. The quantification results show that, on average, the diameter of isolated GBPs changes from 166 to 173 km, then down to 165 km. the maximum intensity contrast changes from 1.012 to 1.027, then down to 1.011. Liu (2018) researched found that for both isolated and non-isolated BPs, the brightness varies from 0.8 to 1.3 times the average background intensity and follows a Gaussian distribution. The lifetimes of BPs follow a lognormal distribution, with characteristic lifetimes of (267 ± 140) s and (421 ± 255) s, respectively. Their size also follows log-normal distribution, with an average size of about (2.15 ± 0.74) × 10^4 km s^{-2} and (3.00 ± 1.31) × 10^4 km s^{-2} for area, and (163 ± 27) km and (191 ± 40) km for diameter, respectively. Saavedra et al. (2021) establishes that areas and diameters of BPs display log-normal distributions that are well fitted by two different components, whereas the velocity vector components follow Gaussians, and the vector magnitude follows a Rayleigh distribution.

In addition to statistical studies of the properties of BPs, there are also studies of similar properties to sunspots or flares. Utz et al. (2016) investigated whether BPs quantities evolved similarly to sunspots during the solar cycle, which revealed that the quantity of BPs close to the equator is coupled to the global solar cycle but shifted in time by about 2.5 year, and after the end of Cycle 23 and at the starting point of Cycle 24, the more active hemisphere changed from south to north. Clear peaks in the detected number of BPs are found at latitudes of about ±7°, in congruence with the positions of the sunspot belts at the end of the solar cycle. Li et al. (2017) found that BPs also have a power-law distribution like flares over a range of scales. Utz et al. (2017) researched suggest that indeed the quantity of BPs at the solar disc centre is correlated to the relative sunspot number, but with the particular feature of showing two different temporal shifts between the decreasing phase of cycle 23 including the minimum and the increasing phase of cycle 24 including the maximum. These studies mainly focus on the similar characteristics of BPs and other solar activities, but there are few related studies.

The above studies on BPs let us understand many statistical characteristics of PBs and the evolution process of some special BPs. However, according to the convective collapse theory (Spruit and Zweibel 1979) and the hot wall model (Rutten et al. 2000; Steiner et al. 2001). The generation process of BPs is that the magnetic field converges into the inter-granular lanes under the continuous extrusion of the granulation structure to form a strong magnetic field. Under the action of magnetic buoyancy, thousands of Gauss magnetic fields are erected in the photosphere to form a magnetic flux tube. When the CH and CN molecular lines and some spectral lines are used to observe the photosphere, the absorption of these absorption lines becomes weak where the strong magnetic field is concentrated, and more photons in the continuous spectrum are allowed to escape from the deep photosphere through the flux tube, which makes the G-band CH line or TiO band brighter and forms BPs. It shows that the activity of BPs is not static, but a dynamic process (Mallia 1968; M. et al. 2003; Rutten et al. 2001; Kiselman et al. 2000). The variation of BPs brightness otherwise reflects the activity inside the flux tube and the aggregation of magnetic fields. The change in quantity reflects the degree of convective collapse.

Obviously, the study on the statistical characteristics of BPs and the evolution process of some special BPs cannot describe the dynamic evolution process of BPs group well. In addition, due to the insufficiency of the detection algorithm, the quantity of BPs in a single frame image is large, the brightness range is wide, and the shape is different. From detection to research methods, there are a number of challenges. Therefore, there are still the following deficiencies in the study of BPs group characteristics.

- The evolution characteristics of BPs group in terms of brightness and quantity are not clear.
- The differences and characteristics of the evolution of quantity and brightness of BPs groups in different regions (quiet and active) are also unclear.

In this paper, we select a pair of the BBSO solar optical telescope high-resolution image sequences in TiO-band of active and quiet regions, and classify BPs brightness into four levels by machine learning clustering method. It focuses on studying and comparing the evolution process of quantity and brightness of groups within four BPs brightness levels in these two different regions in the time dimension.

The layout of the paper is as follows. Section 2 describes the selection of solar telescopes and data. Section 3 describes the BPs detection model. Section 4 describes the data processing methods and results. Section 5 describes the analyzes and discussion . The conclusion are in Sect. 6.

2. Observatory and Data

The data observed by the Goode Solar Telescope (GST) of 1.6 m aperture at Big Bear Solar Observatory (BBSO) were used in our study. GST with adaptive optics (AO), which can correct the atmospheric distortion in real time so that the observed image effect is evident.

Generally, high-contrast BPs can be observed in the G-band (4300 Å) continuum. In addition to the G-band, the spectral line

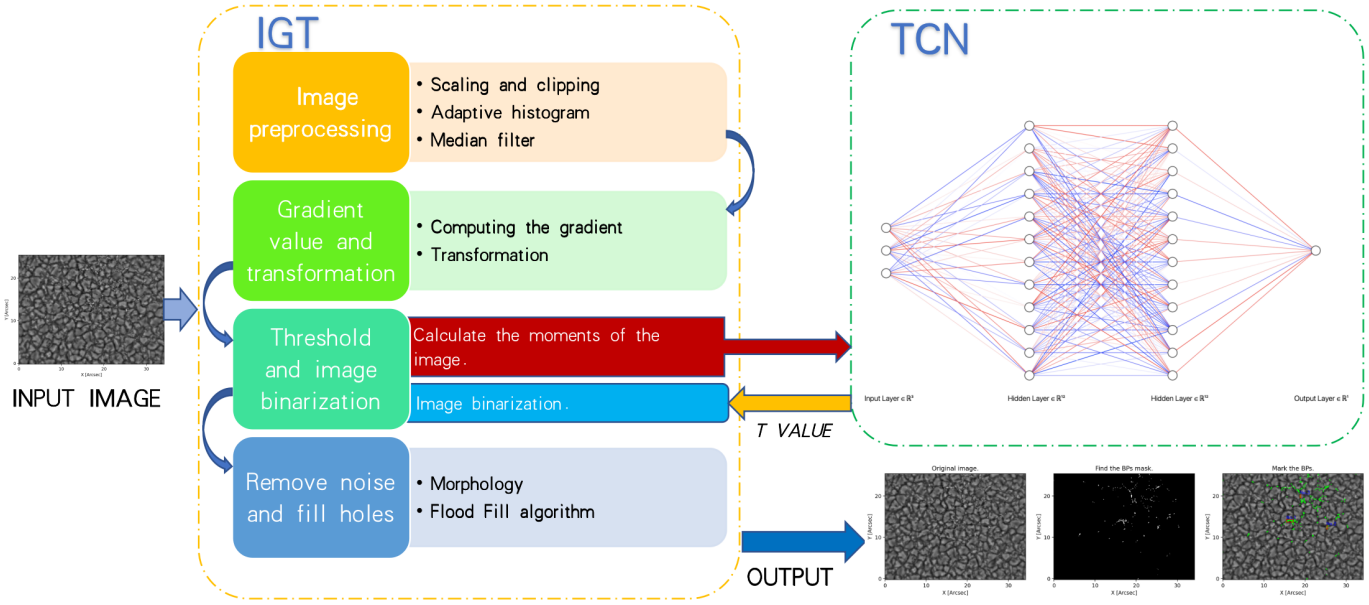

Fig. 1: The structure of HBD Model.

TiO(7058 Å) is also used to observe BPs (Mallia 1968; Liu et al. 2014). TiO (7058 Å) has A longer wavelength than the G-band. The observed range in TiO is better than that in the G-band of ground-based telescopes. We selected data from BBSO from 16:25 to 22:24 on 22 June, 2016 (TARGET: NOAA 12556) and from 16:50 to 22:17 on 30 July, 2020 (TARGET: Quiet sun-Bipolar Region) continuous high quality high-resolution image of Active regions near the center of the solar disk, the former as active region and the latter as quiet region. There were 1501 frames in the active region and 1233 frames in the quiet region. For the sake of one-to-one, we uniformly take the data of the first 1233 frames, a total of 20188.4 seconds (16.4 seconds per frame) , for convenience, the time unit of frames is still used below.

3. Hybrid BPs detection Model (HBD Model)

Due to the problems in the BPs detection algorithm mentioned in Sect. 1, it is challenging to accurately detect BPs with different shapes and brightness in each frame of the observed image sequences. Therefore, we propose a hybrid BPs detection model (HBD Model) that combines Image Gradient Transformation Module (IGT) and Threshold calculation neural network (TCN). Fig. 1 shows the structure of the HBD Model.

The model combines the traditional algorithm based on Laplasian operator with threshold calculation neural network, and uses the powerful fitting ability of neural network to solve the calculation of threshold in the traditional algorithm, improve the robustness of the detection algorithm, so that it has a good detection effect on different observation data and different quality data. At the same time, the model does not need to label image data, each image only needs three values. The problem of image labeling difficulty of deep learning model BPs is avoided. See Fig. 1, IGT contains a series of image processing procedures. IGT and TCN work together in the whole model. The detailed structure and BPs detection process of the model are as follows.

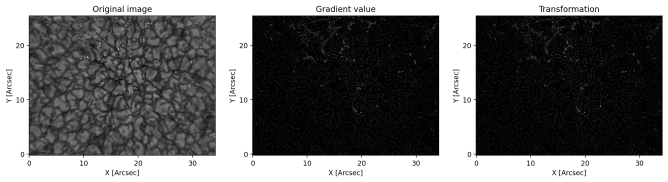

Fig. 2: The results of image gradient calculation and transformation (Step 2).

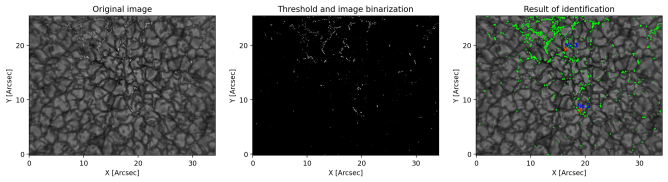

Fig. 3: The results of image Threshold and image binarization (Step 3).

3.1. Image Gradient Transformation Module (IGT)

IGT consists of four steps:

– Step 1. Image preprocessing

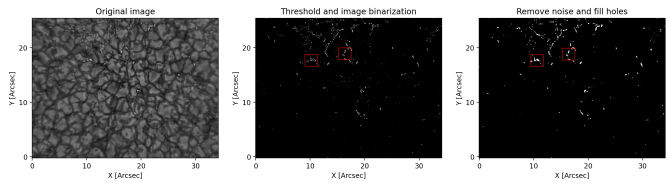

Fig. 4: The results of morphology and Flood FIll Algorithm (Step 4). The red boxes mark the difference before and after the algorithm.

- Step 2. Gradient value and transformation
- Step 3. Threshold and image binarization
- Step 4. Remove noise and fill holes

The following is a detailed description of IGT.

- Step 1. Image preprocessing
  Each pixel value of the original photospheric surface image does not range from 0 to 255, and their span is relatively large. Therefore, the pre-processing stage of the image first needs to scale its data. each pixel value of the image is scaled to 0-255. Meanwhile, due to image edge quality problems, the image was reduced from 2043×2043 pixel to 1000 pixel $\times$ 1000pixel. The formula for image scaling can be defined as:

$$Q = (q - q_{min})/(q_{max} - q_{min}) \tag{1}$$

  Where q is the original pixel value, and q_{max} and q_{min} are the maximum and minimum values of image pixels respectively.Finally, adaptive histogram processing is performed on the scaled image and median filtering is used to remove some stray points.

- Step 2. Gradient value and transformation
  First, We use the Laplace operator to convolve the image to calculate the gradient value of the image. Laplacian operator is a second-order differential operator, which is the second derivative of gray image value (see Gonzalez and Woods 2008). For image $f(x, y)$, it is defined in this work as:

$$\nabla^2 f(x, y) = \partial^2 f(x, y)/\partial x^2 + \partial^2 f(x, y)/\partial y^2 \tag{2}$$

  In this paper, eight adjacent Laplacian operator is used, and the corresponding operator is defined as:

$$\begin{aligned}\nabla^2 f(x, y) = [&f(x+1, y) + f(x+1, y+1) \\ &+ f(x+1, y-1) + f(x-1, y+1) \\ &+ f(x-1, y-1) + f(x-1, y) \\ &+ f(x, y+1) + f(x, y-1)] \\ &- 8f(x, y)\end{aligned} \tag{3}$$

  The filter mask is defined as:

$$L = \begin{bmatrix} -1 & -1 & -1 \\ -1 & 8 & -1 \\ -1 & -1 & -1 \end{bmatrix} \tag{4}$$

  According to the characteristics of Laplace's second order differential operator, the positive and negative values calculated by Laplace correspond to the bright and dark points in the image, and the value of 0 corresponds to the boundary point of the change of gray value. According to the fact that BPs is located in inter-granular lanes, its brightness is brighter than that of its surroundings, which accords with the result of Laplace operator. Of course, this step will contain the wrong BPs, because some of the granulation also have bright points on the edges. Therefore, in the following steps, we also need to remove the wrong BPs.
  Next, we use the image gradient value transformation to enhance the corresponding highlights in the image and remove some unnecessary miscellaneous points. Laplace convolution is the calculation of the second derivative of a grayscale image, and the value of the pixel point is positive or negative. If $f(x_i, y_j)$ represents the pixel value somewhere in the image, we normalize each pixel value to 0 - 255 through the gradient value transformation algorithm and take the absolute value. The algorithm uses the following principles to calculate and process.
  a. if $-255 < f(x_i, y_j) < 0$, else $f(x_i, y_j) =\mid f(x_i, y_j) \mid$
  b. if $f(x_i, y_j) > 255$, else $f(x_i, y_j) = 255$
  c. if $f(x_i, y_j) < 255$, else $f(x_i, y_j) = 255$
  d. if $0 < f(x_i, y_j) < 255$, else $f(x_i, y_j) = f(x_i, y_j)$
  By Laplace convolution and image gradient transformation, the edges of large BPs and small BPs are clearly visible. But there are a lot of gray areas that need to be removed, The result is shown in Fig. 2.

- Step 3. Threshold and image binarization
  We use binarization to remove the gray area of the image so that the bright points in the image can be fully detected. the n-order moments ($N = 1, 2, 3$) of the image are directly calculated and then input into TCN, and the T is calculated by TCN to binarize the image. It should be noted that the TCN requires training prior to this, which we will explain in detail in Sect. 3.2. The result is shown in Fig. 3.

- Step 4. Remove noise and fill holes
  After binarization of the threshold image, BPs is basically recognized. However, some noises are too small, and some middle areas of too large points may produce cavities. This is because the Laplacian convolution calculates the edges of bright points in the image, and the image gradient value transformation steps are not good for holes that are too large. Therefore, morphology is used to remove the small noise points (which are usually on the granulation) and Flood Fill Algorithm is used to fill some large holes. The result is shown in Fig. 4.

3.2. Threshold calculation neural network (TCN)

As mentioned above, The TCN model is a Neural Network model that has been trained and its function is to calculate the threshold T. TCN consists of one input layer, two hidden layers, and one output layer. In the training datasets of TCN, the optimal threshold values of 2678 different images are obtained as the T value of the data set through observation by using IGT alone, and the n-order moments of images ($N = 1, 2, 3$) are calculated as the features of the model.

The reason why the n-order moments of images ($N = 1, 2, 3$) μ, δ and ζ are used as the features of the model is that they represent the average brightness, variance and slope of grayscale images respectively, which comprehensively reflect the grayscale information of different images. Here, we make use of the powerful fitting ability of deep learning to establish some relation-

ship between them and T value , so as to be able to fit the T value of different images well. The calculation formula of these three features is defined as follows:

$$\mu_i = \frac{1}{N}\sum_{j=1}^{N} P_{ij} \tag{5}$$

$$\delta_i == [\frac{1}{N}\sum_{j=1}^{N}(P_{ij}-\mu_i)^2]^{\frac{1}{2}} \tag{6}$$

$$\zeta = [\frac{1}{N}\sum_{j=1}^{N}(P_{ij}-\mu_i)^3]^{\frac{1}{3}} \tag{7}$$

During training, we use 1875 of them as training datasets and 803 as test datasets. The datasets is input into the fully connected neural network to train a deep neural network mode. Finally, the model is used to fit the corresponding thresholds of different images. IGT uses this threshold to binarize images to remove unwanted noises and retain the final BPs. Once the training is completed, IGT only needs to input the three features of the image to TCN, and it can quickly calculate the optimal T value. Table 1 shows the structure of the TCN training data set.

Table 1: The structure of the TCN training datasets.

IMAGE	μ	δ	ζ	T
IMG_1	2.97	4.96	2.906	28
IMG_2	3.8	6.58	3.32	36
$IMG_i(i = 1, 2, ..., N^a)$	.....	.....	.....	.....
IMG_N	3.37	5.459	3.1	32

Notes. [(a)] In this paper, n=1875.

3.3. Experiments

In this paper, in order to test the BPs detection algorithm, the intersection-over-Union (IoU) between the manually labeled BPs image and the image identified by the HBD Model is calculated. This approach is adopted because there is no accepted data set for BPs detection and no accepted algorithm for comparison. At the same time, the scale of BPs is too small, the edges are difficult to determine, some even have only a few pixels, manual labeling will also produce a large error. Therefore, in order to minimize the error caused by manual labeling, three in-line image experts who are very familiar with BPs images were selected in the experiment to label a total of 30 images in three groups (10 images in each group, selected from different observation periods and different quality BBSO images). Each image gets three manually labeled images, and finally the union of the three manually labeled images is taken as the final labeling result. Finally, the IoU is calculated with the image identified by the algorithm.

It is important to note that usually the IoU of an image is calculated as the IoU of the rectangular borders of the two image objects. However, the BPs scale is too small and some of them are long strips with different directions. The image border method has low accuracy for BPs, so this paper uses pixel-level IoU calculation method. The calculation method can be simply described as: First, the image (labelted and identified images) is binarized (0 and 255) and transformed into a matrix; Second, then calculate the sum of the intersection of the two matrices and the sum of the union; Finally, these two sums are used to calculate the final intersection ratio. The pixel-level IoU is more accurate and more sensitive to pixel changes.

Table 2 shows the experimental results, and the value is the average value of each group (10 images). The results show that the IoU of the images recognized by the HBD Model proposed in this paper and the manually lableled images can reach 0.89 on average (The goal is to get close to 1). It has good recognition ability for BPs detection that needs to reach pixel level.

Table 2: Experimental results of BPs detection by HDB Model.

Groups	IoU[a]
$Group_1$	0.90
$Group_2$	0.86[b]
$Group_3$	0.92
Mean	0.89

Notes. [(a)] The value is the average value of each group (10 images). [(b)] Image of active area, not very good quality.

4. Data processing and results

As mentioned above, the aim of this paper is to study the evoltion of BPs groups brightness and quantity in the quiet and active regions. In more detail, we want to investigate how the brightness and quantity of BPs in different brightness levels evolve continuously by focusing on groups of BPs of different brightness rather than individual BPs. Therefore, in this section, we use machine learning clustering method to cluster all BPs brightness values on each frame of continuous image sequences into 4 levels, and each level is regarded as a group. Taking frame as time unit and combining Fourier transform to process and analyze the evolution process of each level.

4.1. BPs detection and brightness calculation

The BHD Model in Sect. 3 is used to detect all BPs frame by frame, and the brightness value I_o is calculated for each BPs on each frame. The calculation formula is defined as:

$$I_o = I_{sb} - I_{bg} \tag{8}$$

Where I_{sb} is the average brightness of A single BPs, and I_{bg} is the average brightness of the current frame. It should be noted that The BPs of the quiet region image sequences can be accurately detected by using the HBD Model, but the active region image sequences cannot be detected simply by using the HBD Model, because it contains sunspots. We first use the HBD Model to detect BPs in the active region, but this will also misidentify the bright filaments in the active region. So let's solve this problem. We directly use the algorithm of Yu et al. (2014) to detect sunspots. We define $S(x, y)$ as the detected sunspot image, $B(x, y)$ as the detected BPs image, and $A(x, y)$ as the final detected result. The calculation formula is defined as:

$$A(x, y) = B(x, y) - S(x, y) \cap B(x, y) \tag{9}$$

The results of the algorithm process are shown in Fig. 5.

4.2. The brightness of clustering

Through the above calculation, we have two Data sets, quiet region Data (Q-DATA) and active region Data (A-DATA), each

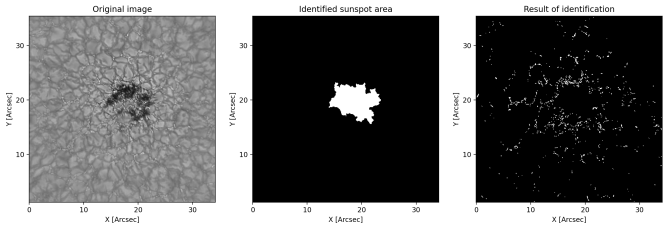

Fig. 5: Results of BPs detection in active region.

containing 1233 frames of Data respectively, and each frame containing several BPs brightness values. we plot the first five frames of Q-DATA and A-DATA. These two datasets have a three-dimensional data structure, including changes in time and space. If we want to understand the evolution of BPs groups in time scale, it is necessary to change the two-dimensional brightness data in each frame into one dimension, so that it can be conveniently combined with the time dimension to analyze its evolution in time. Here, we cannot simply calculate the average brightness of all BPs in each frame to solve this problem. This will make the analysis rough and it is impossible to see the evolution process of brightness and quantity at different levels of brightness. We also cannot artificially specify the brightness level for each frame, because the entire brightness range may vary from frame to frame. Therefore, we adopted the clustering method of machine learning to cluster the brightness data of each frame into 4 levels, namely Level1, Level2, Level3 and Level4 (Level1<Level2<Level3<Level4). They correspond to the set of brightness data from low to high in each frame,and each level represents a brightness group. Fig. 6 shows the effect of clustering the number of the first 100 frames in the active region, it can be seen that the data of each frame is divided into four levels. This ensures that every frame we get the four levels of different brightness correctly.

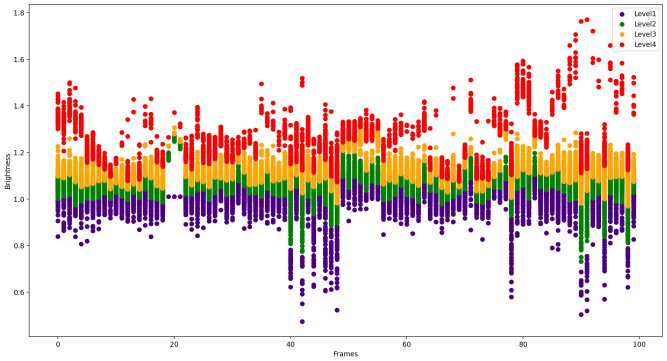

Fig. 6: After clustering the first 100 frames in the active region (The quiet region is similar).

It is worth noting that the reason for dividing the brightness of each frame into four levels is that we find that the brightness distribution on each frame is approximately triangular, with most of it concentrated at the bottom and a few values far larger than the others, far away from the majority. Divided into four levels, most values will be sorted into Level1 or Level2, and other large values will be sorted into Level3 or Level4. If we increase the number of the level, the data at the bottom doesn't matter much, and only the rarer and larger values are affected, which may be divided into smaller levels. This is not good for our research, because these values are very special. On the other hand, if the level is too small, such as 2 or 3 levels, it is not conducive to the reasonable division of brightness level.

After dividing the levels, we calculated the average brightness (hereafter referred to as brightness) and the quantity of BPs of the four different brightness levels in each frame, and then obtained the quantity and brightness of BPs of the four different brightness. Taking the image frame as the X-axis and the brightness or quantity as the Y-axis, the brightness and quantity values in the four brightness levels of all image series frames were plotted respectively, and then the quantity and brightness evolution curves of BPs groups in the four brightness levels of the two data sets were obtained. Fig. 7 shows the BPs quantity evolutions in four different brightness levels in two different regions, where the blue line represents the quiet region and the red line represents the quiet region. Fig. 8 shows the evolution in the brightness of BPs. Detailed analysis and comparison will be provided in Sect. 5.

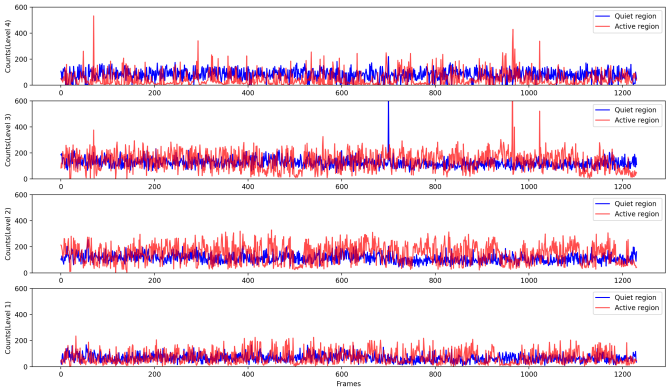

Fig. 7: BPs quantity evolution curves in quiet (blue line) and active regions (red line).

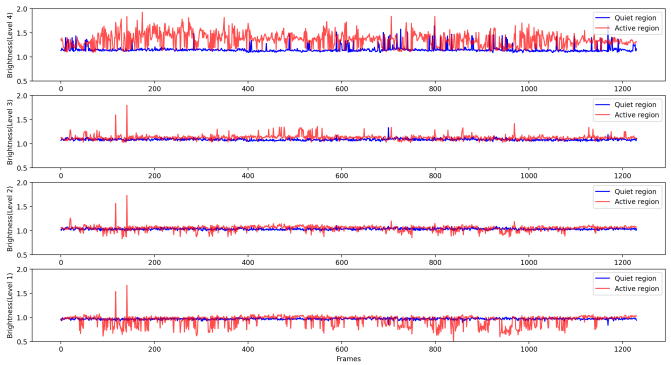

Fig. 8: BPs brightness evolution curves in quiet (blue line) and active regions (red line).

4.3. Evolution curve processing and analysis

In Sect. 4.2, the continuous evolution curves of BPs group quantity and brightness in four different brightness levels of quiet region and active region are calculated and drawn. These curves are very complex, and although we can simply compare the size and scope of their fluctuations, we cannot further understand the internal rules of their changes. Therefore, we want remove noise

and extract the main parts. We perform a fast Fourier transform (FFT) of these quantity and brightness curves, then remove a large amount of DC and frequency noise components, and perform an inverse fast Fourier transform (IFFT) .

We first perform FFT for the quantity curves in four different brightness levels. Figs. 9 and 10 respectively show the BPs group quantity evolution spectra of four brightness levels in the quiet and active regions (level1-Level4 from bottom to top). In order to get the main frequency component, we cut and retain the middle part. In the quiet region Level1-Level2 interception amplitudes range from 2000 to 5000 and Level3-Level4 interception amplitudes range from 1800 to 4000. The interception amplitude ranges of the active region are Level1: 2500-6000, Level2: 3500-6000, Level3: 3800-6000, and Level4: 2800-6000. After obtaining the results of the Fourier transform (FFT), we intercept the main frequency component and then perform the inverse Fourier transform (IFFT). Figs. 11 and 12 show the result of the inverse Fourier transform. It should be noted that the basis of such interception is to remove DC components and noise components as much as possible by observing FFT images, and slight deviation will not cause too much influence on the results.

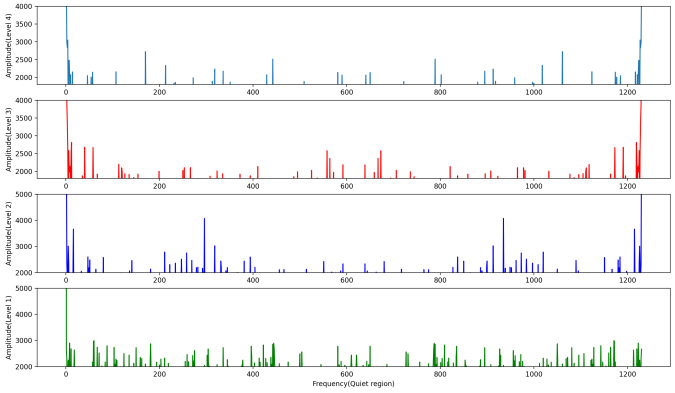

Fig. 9: FFT of evolution curve of BPs quantity in quiet region.

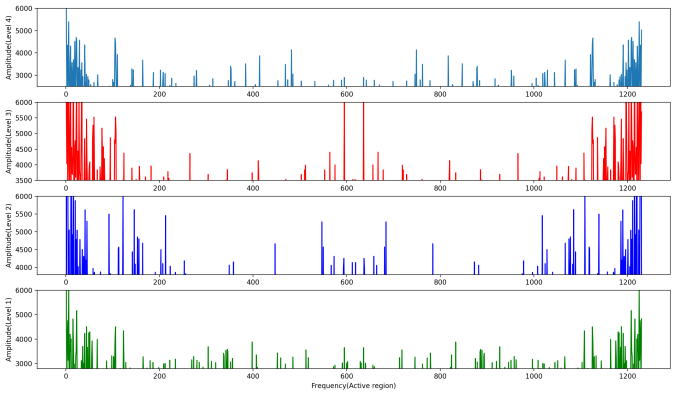

Fig. 10: FFT of evolution curve of BPs quantity in active region.

In the same way, we also make FFT and IFFT for BPs group brightness evolution curves of level1-Level4 in different brightness levels. Figs. 13 and 14 are FFT results, and Figs. 15 and 16 are IFFT results. In the quiet region, the interception amplitude range Level1-Level3 are 1-2, and Level are 3-8. The interception amplitude range of the active region is Level1: 5-12, Level2: 2.5-7, Level3: 2.5-7, Level4: 7-15.

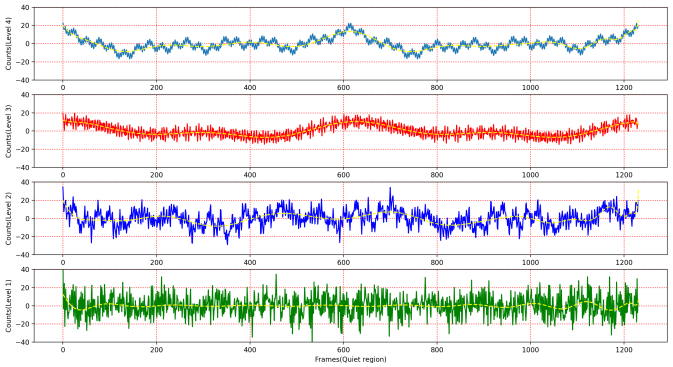

Fig. 11: IFFT of evolution curve of BPs quantity in quiet region.

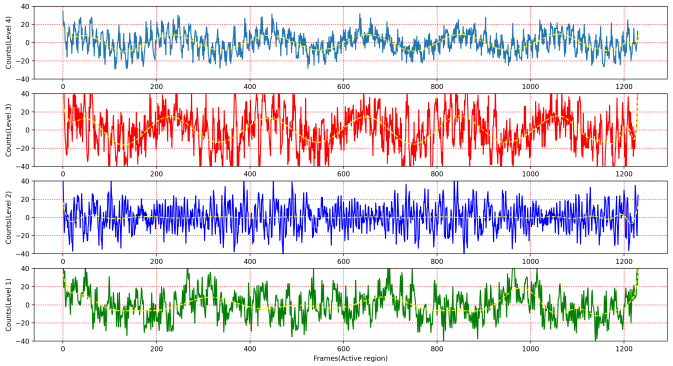

Fig. 12: IFFT of evolution curve of BPs quantity in active region.

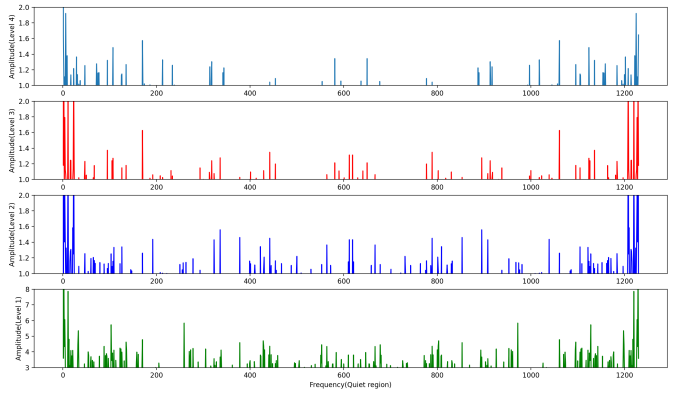

Fig. 13: FFT of evolution curve of BPs brightness in quiet region.

5. Analysis and discussion

5.1. Analysis of BPs group quantity and brightness curve evolution characteristics in quiet and active regions

From Fig. 7, it can be easily found that from Level1 to Level4, the blue line (quiet region) is all wrapped in the red line (active region), indicating that the quantity of BPs in the active region (red line) changes more sharply than that in the quiet region (blue line), and indicating that compared with the quiet region, the birth and death of BPs in the active region are faster, and the convective collapse process is more active. In the quiet region, Level1-Level3 quantity changes are relatively stable, while Level4 quantity changes are more drastic than the other three levels. This indicates that the brighter BPs in the quiet region are

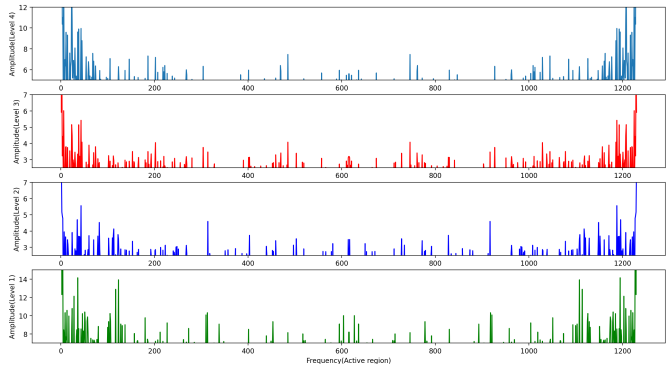

Fig. 14: FFT of evolution curve of BPs brightness in active region.

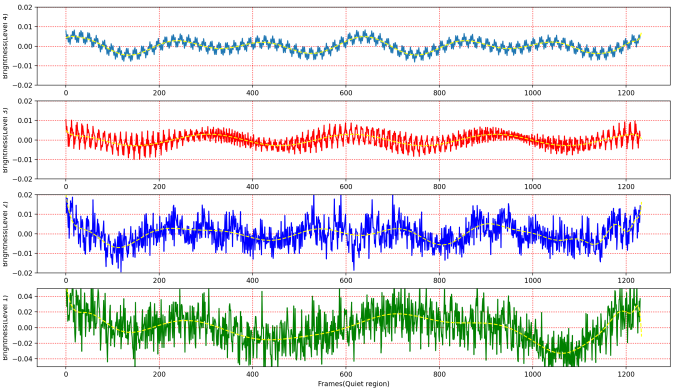

Fig. 15: IFFT of evolution curve of BPs brightness in quiet region.

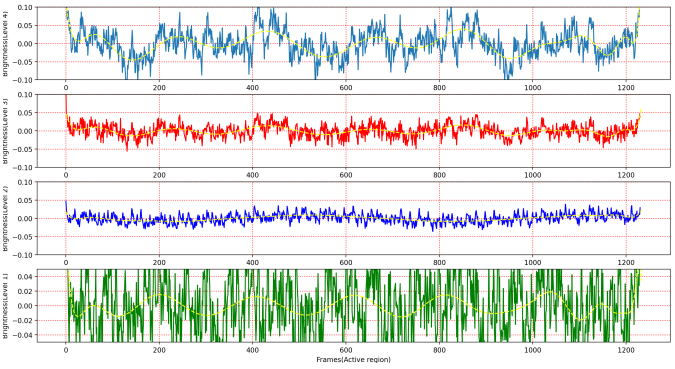

Fig. 16: IFFT of evolution curve of BPs brightness in active region.

more active. From Level1 to Level4, the quantity curve of the active region shows more and more violent fluctuations. Level4 also shows that the overall fluctuation is larger than that of the quiet region, but the overall curve moves down, that is, the lowest point of the curve is close to 0. This indicates that the quantity of PBs in the active region decreases sharply at Level4, which has the highest brightness, and even approaches 0. But at the same time, Level4 in the active zone, it's going to have a sudden change in its quantity. It indicates that a large number of BPs of this brightness Level will be generated in a short time, that is, the BPs of medium and low brightness will turn into the BPs of high brightness in a short time, but disappear in a short time. This indicates that the magnetic elements in the active region gather very quickly, gathering together in a short time and disappearing in a short time. It is possible that the convection of granulation in the active region is more rapid, which promotes the accelerated accumulation and disappearance of magnetic elements in the lane, resulting in the sudden change of BPs high brightness Level4.

On the other hand, by observing the BPs group brightness evolution curve of the four brightness levels in Fig. 8, it can be clearly found that the overall brightness of the four levels in the quiet region does not change much, except for Level4, which is more drastic. At the same time, the changes of Level2 and Level3 in the two regions are basically the same, without particularly drastic changes. It indicates that in the middle brightness Level, there is little difference between the changes of BPs brightness in the two regions, and there is no drastic fluctuation. But Level1 and Level4 in the activity region show a completely different situation. In Level1, the brightness change of the active region is more drastic than that of the quiet region, but generally lower than that of the quiet region. In Level4, the brightness changes in the active region are more dramatic than those in the quiet region, but generally higher than those in the quiet region. In general, among the four brightness levels, BPs group brightness changes in the quiet region show a relatively stable situation, except for a slightly drastic change in the highest brightness Level. However, in the active region, the changes of low brightness and brightness Level were more dramatic, and the intermediate Level was also relatively stable.

According to the observation and analysis of Figs. 7 and 8, we can find that the BPs in the active region is more active than that in the quiet region, and the rate of birth and death is faster, and this situation becomes more obvious with the increase of brightness. In addition, the quiet region showed steady activity across the four different brightness levels, with the exception of Level4, which was slightly more intense. In active region, the low brightness Level and high brightness Level fluctuated sharply. For a clearer explanation, we calculated the average maximum, average minimum, mean, variance, standard deviation and median of the four brightness levels in the two regions (as shown in Table 3). It is also easy to see the difference between quiet and avtive regions, and the BPs brightness in the active region is generally larger than that in the quiet region. This indicates that the solar activity in active region has a great influence on the activity of PBs.

5.2. Analysis of FFT and IFFT characteristics of quantity evolution curves of BPs groups in quiet and active regions

It can be seen from Figs. 9 and 10 that the frequency component in the active region is more than that in the quiet region, and there are more frequency components near the DC component. At the same time, the clutter range of each level is not the same, so the frequency range of each level is not the same. After removing a large number of DC components and noise frequency components, the IFFT image of the remaining main frequency components enables us to understand more clearly the characteristics of BPs group number variation in the two regions.

The IFFT curves of the quantity of groups in Fig. 11 and 12 show very interesting properties. Level1 of the two regions does not have too many periodic changes, except that the active region fluctuates sharply. Indicates that two region in the evolution of the low number of BPs brightness is nothing what regularity, in

Table 3: Comparison of maximum, minimum and mean values of four brightness levels in quiet and active regions.

Region	Values	Level1	Level2	Level3	Level4
Quiet region	Max[a]	0.998	1.057	1.114	1.221
	Min	0.893	1.001	1.057	1.123
	Mean	0.968	1.031	1.085	1.151
	Var	0.0006	0.0003	0.0002	0.0005
	Std	0.024	0.016	0.015	0.021
	Median	0.974	1.032	1.084	1.147
Active region	Max[b]	0.992	1.086	1.209	1.455
	Min	0.816	0.999	1.091	1.307
	Mean	0.943	1.049	1.127	1.351
	Var	0.0021	0.0007	0.0007	0.0014
	Std	0.041	0.023	0.026	0.034
	Median	0.954	1.051	1.123	1.344

Notes. [(a)] The average value of the maximum value of the different levels in each frame. Other values are calculated similarly. [(b)] Refer to the calculation method of Max of quiet region.

the random fluctuations, also demonstrated the low brightness of BPs life shorter, more unstable, many BPs may have not reached a certain brightness, the magnetic field also converge to a certain degree was at the end of the extrusion of granulation or other reasons and disappeared. However, from Level2 to Level4, the two regions show certain regular characteristics. The following detailed analysis compares the evolution characteristics of the two regions.

Figure. 11 shows that level2 shows no change pattern in the quiet region, but Level3 and Level4 show relatively uniform evolution characteristics, with both showing a peak around frame 612 (10036.8 s) and then slowly declining thereafter. At the same time, these two levels show the characteristics of large changes, and at the same time contain small periodic evolution rules. Level3 has a period of approximately 410 ± 32.8 s (25 ± 2 frames), an amplitude of approximately 8 ± 2, and a small period evolution in the shape of a sausage wave. Level4 also contains an open-down half-wave small periodic evolution with a period of 410 ± 32.8 s (25 ± 2 frames) and an amplitude of approximately 10 ± 2.

According to the IFFT evolution curve of the quantity of groups in the active region in Fig. 12, except for Level1, all the three levels show certain evolution periodic characteristics. Level2 shows sausage-like change characteristics with a period of about 5740 ± 82 s (350 ± 5 frames), but it is not very clear. Although Level3 and Level4 fluctuate sharply, the evolution characteristics of periodicity can be clearly obtained through the fitting curve. Moreover, both levels show the characteristics of periodic 3280 ± 5 s (200 ± 5 frames), but the amplitudes of Level3 are 14 ± 2 and Level4 are 8 ± 1.

By analyzing the evolution characteristics of the quantity of groups in the four brightness levels in the two regions of BPs, it can be found that the evolution of BPs in the low brightness levels of the two regions is not regular at all, but the evolution rules from Level2 to Level4 are all certain, and Level3 and Level4 even have periodic characteristics. This indicates that when the brightness of PBs is relatively bright and the stability is relatively stable, the evolution of the quantity of PBs groups has a certain regularity, but is not chaotic.

5.3. Analysis of FFT and IFFT characteristics of brightness evolution curves of BPs groups in quiet and active regions.

Figures. 13 and 14 show the FFT of BPs group brightness evolution curves at four levels of different brightness regions. Similar to the group quantity evolution FFT, in order to obtain the main frequency components, the four Level interception frequencies of the FFT brightness evolution curve in the active region are all different. At the same time, there are also many frequency components near the DC component in the active region. This indicates that there are more stable BPs groups in the active region than in the quiet region.

The IFFT of BPs group brightness evolution curve with four different brightness levels is completely different from the IFFT of BPs group quantity evolution curve.

Firstly, we analyze the group brightness evolution curve IFFT of the quiet region in Fig. 13. It can be found from the figure that Level1 and Level2 have no law at all, showing a completely random fluctuation state, and the curve fitting also looks down on any law. Levels 3 and 4, however, show a clear periodic pattern. Both of these are big periodic changes with some small periodic changes, Level3 has even more complex periodic changes in amplitude. Level3 shows a period evolution of about 5084 ± 82 s (310 ± 5 frames) with an amplitude of about 0.0032. In addition, Level3 contains some small periodic changes, with periodic periods and amplitudes shrinking and growing. Level4, on the other hand, shows a periodicity of about 3526 ± 82 s, with amplitudes decreasing and increasing every 8200 s. At the same time, the large periodic change of Level also includes the small periodic change with a period of about 328 ± 32.8 s (20 ± 2 frames) and an amplitude of about 0.0045 ± 0.0025.

The group brightness evolution of the active region is quite different from that of the quiet region. From the observation of Fig. 14, it can be found that the evolution of Level3 and Level4 in the active region is irregular, indicating that the group variation characteristics of high brightness and brightness in PBs in the active region are completely random. Level1 has obvious periodic changes. Although the waveform is very sharp, it can be seen from the fitting curve, showing a period of 3280 ± 164 s (200 ± 10 frames) and an amplitude of 0.0097 ± 0.001. Level2 has a large fluctuation throughout the observation period, but a complete set of periodic changes cannot be observed.

In general, among different brightness levels, BPs in the quiet region shows no periodicity in the evolution of group brightness in the low brightness level (Level1 or Level2), while BPs in the medium and high brightness level (Level3 or Level4) shows very rich periodicity, indicating that BPs in the quiet region has certain periodic characteristics after its brightness is stable. However, BPs in the active region has no other levels except for the periodicity of the group brightness evolution in the low brightness. This indicates that the brightness characteristics of BPs groups in the active region are completely random. On the other hand, its activity is very active and unstable.

6. Conclusion

In this paper, We propose a PBs hybrid detection model (HBD Model), which combines the advantages of traditional algorithms and neural networks. On this basis, we detect and calculate the brightness value of each BPs in each frame of the image series in the quiet and active regions. They are divided into four levels by machine learning clustering method, and the characteristics of brightness and number evolution of BPs groups in

these four levels are analyzed by FFT (Fourier transform) IFFT (Inverse Fourier transform).

The main results of this paper are summarized as follows.

1. Compared with the quiet region, the BPs in the active region were more active, and the changes of the brightness and quantity of BPs groups were more drastic. At the same time, the medium and low brightness BPs in the active region evolved into the high brightness BPs more quickly and died out quickly.
2. The quantity evolution of BPs groups in the quiet region and the active region had certain periodic evolution characteristics at Level3 and Level4 of medium and high brightness. Level1 is in random fluctuations. Among them, Level3 and Level4 both show a clear peak and contain a small periodic change. The small periodic change contained in Level3 is the shape of sausage wave. Activity regions Level3 and Level4 show obvious periodic changes. At the same time, Level2 shows a sausage wave period change with relatively large amplitude.
3. At different brightness levels, the evolution characteristics of BPs group in quiet region are more regular than those in active region. The evolution characteristics of the group brightness and the quantity of groups in the quiet region show very interesting characteristics, which are characterized by small periodic changes in the large periodic changes. However, the evolution characteristics of the brightness of the active region group showed a random drastic fluctuation except for the low brightness Level1, which showed a unclear periodic change.

Based on the above conclusions, we further understand the characteristics of BPs. BPs in active region are more active than in quiet region, birth and death occur more quickly, and brightness changes more quickly. On the other hand, the magnetic field activity of small magnetic elements in active region is more abundant and active. They may contribute to the accumulation of magnetic flux energy in surrounding solar events (e.g., sunspots, flares), and also carry some of the magnetic flux energy further through the magnetic flux tube into the chromosphere or corona. In summary, BPs activity is related to other solar events, and they may directly or indirectly influence or be influenced by larger solar events,such as flare or sunspots and so on.

The activities of BPs groups are not random and disorderly (although individually they look very random). In the quiet and active regions, the evolution of the quantity of BPs groups at the stable medium-high brightness Level and the evolution of the groups brightness at this Level showed clear evolution characteristics. The periodicity of group brightness and quantity changes in different brightness levels of quiet and active regions is more effective for us to understand the activity of BPs, and enables us to have a new understanding of the characteristics of BPs as a whole, instead of only focusing on a few special BPs. Further research into the periodicity of BPs activity will help predict BPs activity in the future, which in turn will help predict other solar events, such as flares.

In this study, we selected a pair of observations in quiet and active regions to study, made a preliminary exploration of the BPs detection algorithm and the research methods and characteristics of group evolution, and obtained some characteristics of BPs evolution. However, further research is needed to find out the universal evolution characteristics of BPs group evolution, which will be further carried out in the future research.

Acknowledgements. We gratefully acknowledge the use of data from the Goode Solar Telescope (GST) of the Big Bear Solar Observatory (BBSO). BBSO operation is supported by US NSF AGS-1821294 grant and New Jersey Institute of Technology. GST operation is partly supported by the Korea Astronomy and Space Science Institute and the Seoul National University.

References

A., A., van, Ballegooijen, M., Asgari-Targhi, S., R., Cranmer, and, 2011. HEATING OF THE SOLAR CHROMOSPHERE AND CORONA BY ALFVN WAVE TURBULENCE. The Astrophysical Journal 736, 3–3.

Berger, T., Schrijver, C., Shine, R., Tarbell, T., Scharmer, G., others, 1995. New observations of subarcsecond photospheric bright points. Technical Report. American Astronomical Society.

Berger, T.E., Löfdahl, M.G., Shine, R.A., others, 1998. Measurements of solar magnetic element dispersal. The Astrophysical Journal 506, 439. Publisher: IOP Publishing.

Berger, T.E., others, 1996. On the dynamics of small-scale solar magnetic elements. The Astrophysical Journal 463, 365.

Colak, T., Qahwaji, R., 2009. Automated Solar Activity Prediction: A hybrid computer platform using machine learning and solar imaging for automated prediction of solar flares: AUTOMATED PREDICTION OF SOLAR FLARES. Space Weather 7, n/a–n/a. URL: http://doi.wiley.com/10.1029/2008SW000401, doi:.

Crockett, P.J., Jess, D.B., Mathioudakis, M., Keenan, F.P., 2009. Automated detection and tracking of solar magnetic bright points. Monthly Notices of the Royal Astronomical Society 397, 1852–1861. URL: https://academic.oup.com/mnras/article-lookup/doi/10.1111/j.1365-2966.2009.15083.x, doi:.

Crockett, P.J., Mathioudakis, M., Jess, D.B., Shelyag, S., Keenan, F.P., Christian, D.J., 2010. THE AREA DISTRIBUTION OF SOLAR MAGNETIC BRIGHT POINTS 722, 6.

De Pontieu, B., 2002. High-resolution observations of small-scale emerging flux in the photosphere. The Astrophysical Journal 569, 474. Publisher: IOP Publishing.

Deng, L., 2017. Automatic detection and extraction of ultra-fine bright structure observed with new vacuum solar telescope, in: Eighth international conference on graphic and image processing (ICGIP 2016), pp. 36–41. Tex.organization: SPIE.

Fedun, V., Shelyag, S., Erdélyi, R., 2010. Numerical modeling of footpoint-driven magneto-acoustic wave propagation in a localized solar flux tube. Astrophysical Journal 727, –.

Feng, S., Ji, K.f., Deng, H., Wang, F., Fu, X.d., 2012. Automatic detection and extraction algorithm of inter-granular bright points. Journal of the Korean Astronomical Society 45, 167–173. Publisher: The Korean Astronomical Society.

Gao, Y., Li, F., Li, B., Cao, W., Song, Y., Tian, H., Guo, M., 2021. Possible Signature of Sausage Waves in Photospheric Bright Points. Solar Physics 296, 184. URL: http://arxiv.org/abs/2112.11756, doi:. arXiv:2112.11756 [astro-ph].

Gonzalez, R., Woods, R., 2008. Digital image processing.

Jess, D.B., Mathioudakis, M., Erdélyi, R., Crockett, P.J., Keenan, F.P., Christian, D.J., 2009. Alfvén waves in the lower solar atmosphere. Science (New York, N.Y.) 323, 1582–1585. Publisher: American Association for the Advancement of Science.

Keys, P.H., Mathioudakis, M., Jess, D.B., Shelyag, S., Crockett, P.J., Christian, D.J., Keenan, F.P., 2011. THE VELOCITY DISTRIBUTION OF SOLAR PHOTOSPHERIC MAGNETIC BRIGHT POINTS. The Astrophysical Journal 740, L40. URL: https://iopscience.iop.org/article/10.1088/2041-8205/740/2/L40, doi:.

Keys, P.H., Reid, A., Mathioudakis, M., Shelyag, S., Henriques, V.M., Hewitt, R.L., Del Moro, D., Jafarzadeh, S., Jess, D.B., Stangalini, M., 2020. High-resolution spectropolarimetric observations of the temporal evolution of magnetic fields in photospheric bright points. Astronomy & Astrophysics 633, A60. Publisher: EDP Sciences.

Kiselman, D., Rutten, R.J., Plez, B., 2000. The formation of G-band bright points. I: Standard LTE modelling. Proceedings of the International Astronomical Union 203.

Li, X., Yang, Z., Zhang, H., Observatories, Y., 2017. Temporal variations of the power-law distribution of low-chromospheric bright points in a solar active region. Astronomical Research & Technology .

Liu, Y., 2018. Studies of Isolated and Non-isolated Photospheric Bright Points in an Active Region Observed by the New Vacuum Solar Telescope. The Astrophysical Journal , 17.

Liu, Z., Xu, J., Gu, B.Z., Wang, S., You, J.Q., Shen, L.X., Lu, R.W., Jin, Z.Y., Chen, L.F., Lou, K., others, 2014. New vacuum solar telescope and observations with high resolution. Research in Astronomy and Astrophysics 14, 705. Publisher: IOP Publishing.

M., Schüssler, S., Shelyag, S., Berdyugina, A., V?gler, and, S., 2003. Why solar magnetic flux concentrations are bright in molecular bands. Astrophysical Journal Letters .

Mallia, E.A., 1968. A study of weak molecular and atomic lines in the photospheric spectrum 5, 281–302.

Mumford, S.J., Erdélyi, R., 2015. Photospheric logarithmic velocity spirals as MHD wave generation mechanisms. Monthly Notices of the Royal Astronomical Society , 2.

Mumford, S.J., Fedun, V., Erdélyi, R., 2015. Generation of magnetohydrodynamic waves in low solar atmospheric flux tubes by photospheric motions. Astrophysical Journal 799, 6.

Rutten, R.J., Kiselman, D., Voort, L.R.v.d., Plez, B., 2000. Proxy magnetometry of the photosphere: why are G-band bright points so bright? Advanced Solar Polarimetry-Theory, Observation, and Instrumentation .

Rutten, R.J., Kiselman, D., Voort, L.R.V.D., Plez, B., 2001. Proxy magnetometry of the photosphere: why are G-band bright points so bright? Advanced Solar Polarimetry – Theory, Observation, and Instrumentation 236.

Saavedra, G.B., Utz, D., Dominguez, S.V., Rozo, J., Manrique, S., Gömöry, P., Kuckein, C., Balthasar, H., Zelina, P., 2021. Observational evidence for two-component distributions describing solar magnetic bright points. arXiv preprint arXiv:2110.12404 .

Spruit, H., Zweibel, E., 1979. Convective instability of thin flux tubes. Solar Physics 62, 15–22. Publisher: Springer.

Steiner, O., Hauschildt, P., Bruls, J., 2001. Radiative properties of magnetic elements-I. Why are-band bright points bright? Astronomy & Astrophysics 372, L13–L16. Publisher: EDP Sciences.

Utz, D., Muller, R., Doorsselaere, T.V., 2017. Temporal relations between magnetic bright points and the solar sunspot cycle. Publications of the Astronomical Society of Japan 69, 12.

Utz, D., Muller, R., Thonhofer, S., Veronig, A., Hanslmeier, A., Bodnárová, M., Bárta, M., del Toro Iniesta, J., 2016. Long-term trends of magnetic bright points-I. Number of magnetic bright points at disc centre. Astronomy & Astrophysics 585, A39. Publisher: EDP Sciences.

Vigeesh, G., Fedun, V., Hasan, S.S., Erdélyi, R., 2012. Three-dimensional simulations of magnetohydrodynamic waves in magnetized solar atmosphere. The Astrophysical Journal 755, 18–18.

Xiong, J., Yang, Y., Jin, C., Ji, K., Feng, S., Wang, F., Deng, H., Hu, Y., 2017. The characteristics of thin magnetic flux tubes in the lower solar atmosphere observed by hinode/SOT in the G band and in Ca II H bright points. The Astrophysical Journal 851, 42. Publisher: IOP Publishing.

Xu, L., Yang, Y., Yan, Y., Zhang, Y., Bai, X., Liang, B., Dai, W., Feng, S., Cao, W., 2021. Research on multiwavelength isolated bright points based on deep learning. The Astrophysical Journal 911, 32. Publisher: IOP Publishing.

Yang, Y., Li, Q., Ji, K., Feng, S., Deng, H., Wang, F., Lin, J., 2016. On the relationship between G-band bright point dynamics and their magnetic field strengths. Solar Physics 291, 1089–1105.

Yang, Y.F., Li, X., 2019. Morphological Classification of G-band Bright Points Based on Deep Learning. The Astrophysical Journal 887, 129 (10pp).

Yang, Y.F., Lin, J.B., Feng, S., Ji, K.F., Deng, H., Wang, F., 2014. Evolution of isolated G-band bright points: size, intensity and velocity , 13.

Yu, L., Deng, L., Feng, S., 2014. Automated sunspot detection using morphological reconstruction and adaptive region growing techniques, in: Proceedings of the 33rd Chinese Control Conference, IEEE. pp. 7168–7172.